

$K_3Fe(CN)_6$ under External Pressure: Dimerization of CN^- Coupled with Electron Transfer to Fe(III)

Kuo Li,^{*,†,‡} Haiyan Zheng,^{*,†,‡} Lijuan Wang,[†] Christopher A. Tulk,[§] Jamie J. Molaison,[§] Mikhail Feyngenson,[§] Wenge Yang,^{†,||} Malcolm Guthrie,[‡] and Hokwang Mao^{†,‡}

HPSTAR
2015-118

[†]Center for High Pressure Science and Technology Advanced Research, Beijing 100094, P. R. China

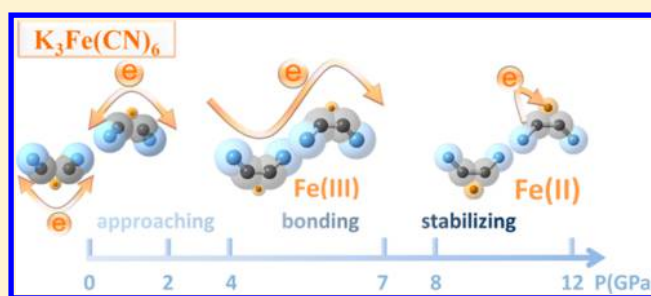
[‡]Geophysical Laboratory, Carnegie Institution of Washington, Washington, D.C. 20015, United States

[§]Neutron Sciences Directorate, Oak Ridge National Laboratory, Oak Ridge, Tennessee 37830, United States

^{||}HPSynC, Geophysical Laboratory, Carnegie Institution of Washington, Argonne, Illinois 60439, United States

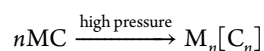
S Supporting Information

ABSTRACT: The addition polymerization of charged monomers like $C\equiv C^{2-}$ and $C\equiv N^-$ is scarcely seen at ambient conditions but can progress under external pressure with their conductivity significantly enhanced, which expands the research field of polymer science to inorganic salts. The reaction pressures of transition metal cyanides like Prussian blue and $K_3Fe(CN)_6$ are much lower than that of alkali cyanides. To figure out the effect of the transition metal on the reaction, the crystal structure and electronic structure of $K_3Fe(CN)_6$ under external pressure are investigated by *in situ* neutron diffraction, *in situ* X-ray absorption fine structure (XAFS), and neutron pair distribution functions (PDF) up to ~15 GPa. The cyanide anions react following a sequence of approaching–bonding–stabilizing. The Fe(III) brings the cyanides closer which makes the bonding progress at a low pressure (2–4 GPa). At ~8 GPa, an electron transfers from the CN to Fe(III), reduces the charge density on cyanide ions, and stabilizes the reaction product of cyanide. From this study we can conclude that bringing the monomers closer and reducing their charge density are two effective routes to decrease the reaction pressure, which is important for designing novel pressure induced conductor and excellent electrode materials.



INTRODUCTION

With the strong driving force provided by external pressure, unsaturated species tend to crystallize (for liquid) and polymerize in the solid state without solvent or catalyst.^{1–7} This is defined as pressure-induced polymerization (PIP). The monomers of PIP include not only neutral molecules but also charged ions like metal cyanides^{8,9} and acetylides.^{10,11} The polymerization products of cyanides or acetylides usually contain conjugated double bonds, which are expected to be conductive. The conjugated skeleton bonds to the embedded metallic cations directly, and the pre-existing properties of the metallic cations will be strongly coupled with the conductive carbon skeleton, which may produce extraordinary physical and chemical properties. The reaction process can be summarized in the following equation:



where M stands for metal cations, C for the unsaturated carbon or carbon-based groups, and $[C_n]$ for the carbon-based network.

The PIP of metal cyanides is specially focused due to its potential application on the electrode materials, as reported in the Prussian blue compounds.^{12,13} Metal cyanides are economic

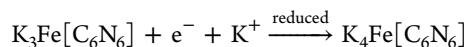
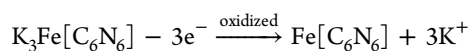
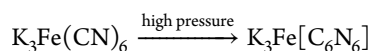
materials, but most of them are insulators and can only transform to conductors after polymerization. As is well-known, the polymerization of simple metal cyanides (including ACN, A = Na, K, Rb, Cs) usually occurs at tens of GPa,^{8,9,14} too high for industrial applications, while the transition metal cyanides like Prussian blue^{15–18} were reported to react at several GPa. Since a low reaction pressure is of great significance for industrial applications, the effect of metal cations on the bonding process and the corresponding conductivity need to be investigated.

$K_3Fe(CN)_6$ is a good model compound with its PIP starting between 2 and 4 GPa, which is one of the lowest reaction pressures of CN^- .¹⁹ The CN^- anions bond to Fe(III) and K^+ at carbon and nitrogen atom, respectively, with which we can compare the effect of alkali metal (K) and transition metal (Fe) on the PIP in one compound. Additionally, the PIP product of $K_3Fe(CN)_6$ is expected to be conductive and electrochemically active, which has potential applications as the cathode of rechargeable alkaline batteries, as proposed in the following equations.

Received: July 15, 2015

Revised: September 6, 2015

Published: September 14, 2015



$\text{K}_3\text{Fe}(\text{CN})_6$ undergoes three phase transitions upon compression up to ~ 15 GPa, as identified with the *in situ* X-ray diffraction (XRD) and Raman spectroscopy: phase O1 to phase O2 (O for orthorhombic) at 2–4 GPa, phase O2 to phase O3 at 7–8 GPa, and the amorphization of phase O3 at around 12 GPa.¹⁹ The transitions are accompanied by bonding between cyanide anions (identified by Raman spectroscopy) and 10³-fold enhancement of electrical conductivity at 2–4 GPa and a decrease at 7–8 GPa. In this paper, to understand the reaction process and the effect of metal cations, as well as the variation of the conductivity, we determined the crystal structure of $\text{K}_3\text{Fe}(\text{CN})_6$ and the electronic structure of Fe before and after the reaction using *in situ* neutron diffraction and X-ray absorption fine structure (XAFS). We discovered the bonding between CN and reduction of Fe(III) to Fe(II) under high pressure. Combining with the results of neutron pair distribution function (PDF) analysis on the recovered sample, we also found that the irreversible bonding between CN is closely related to the donation of electrons from CN to Fe(III). From this research we can conclude that in $\text{K}_3\text{Fe}(\text{CN})_6$ the bonding between cyanides includes three steps under high pressure: approaching (of $\text{C}\equiv\text{N}^-$), bonding (between $\text{C}\equiv\text{N}$), and stabilizing (of the product). The Fe cations bring the coordinated CN^- closer to each other at a distance significantly below the sum of van der Waals radii, which facilitates the bonding process. The donation of electrons from CN to Fe(III) helps to reduce the charge density on CN and stabilize the product.

EXPERIMENTAL SECTION

Sample Preparation. A fine powder of $\text{K}_3\text{Fe}(\text{CN})_6$ (orthorhombic phase, Sigma-Aldrich, particle size < 10 μm), which was gently ground in an agate mortar for less than 5 min, was used for the *in situ* neutron powder diffraction and XAFS measurements. This was also used for the synthesis of the compressed $\text{K}_3\text{Fe}(\text{CN})_6$ for the neutron PDF measurements. These samples were synthesized at beamline-3 Spallation Neutrons and Pressure Diffractometer (SNAP), spallation neutron source (SNS), Oak Ridge National Lab (ORNL). For the samples recovered from below 5 GPa, $\text{K}_3\text{Fe}(\text{CN})_6$ (151 mg) was prepressed into a pellet and then placed into the VX3 Paris-Edinburgh (PE) Press with WC anvils. For the samples recovered from 6 to 20 GPa, 54 mg of $\text{K}_3\text{Fe}(\text{CN})_6$ was prepressed into a pellet and the VX3 Paris-Edinburgh (PE) Press with sintered diamond anvils was used.²⁰ The system was driven by an automatic hydraulic oil syringe pump with the pressure calibrated previously. All the samples were kept at the target pressure for about 1 h and then slowly downloaded to ambient pressure.

In Situ Neutron Diffraction. *In situ* neutron diffraction patterns were collected at the SNAP beamline, at the SNS, ORNL. A VX3 Paris-Edinburgh press equipped with sintered-diamond double-toroidal anvils with a null-scattering titanium zirconium (TiZr) alloy gasket was used for applying pressure. The mixture of CD_3OD and $\text{C}_2\text{D}_5\text{OD}$ ($\text{CD}_3\text{OD}:\text{C}_2\text{D}_5\text{OD} = 4:1$) was used as a pressure medium. The pressure was

calibrated by the unit cell volume–pressure curve that was determined by *in situ* X-ray diffraction (XRD) data and ruby fluorescence.

PDF Measurements. The neutron PDF data of the samples recovered from various pressures were collected at the Nanoscale-Ordered Materials Diffractometer (NOMAD), SNS, ORNL.²¹ Neutron scattering up to $Q_{\text{max}} = 2\pi/d = 31.41 \text{ \AA}^{-1}$ was used for PDF analysis.

XAFS Measurements. The $\text{K}_3\text{Fe}(\text{CN})_6$ prepared by the method described above was loaded into a symmetric-style diamond anvil cell (DAC) fitted with nanocrystalline diamonds polished to a culet diameter of $d_{\text{culet}} = 400 \mu\text{m}$. T301 stainless steel gaskets were preindented to a thickness of $\sim 30 \mu\text{m}$, and holes with $d = 200 \mu\text{m}$ were drilled in the center of the indentation to serve as the sample chamber. Neon was loaded as the pressure medium using the GSECARS gas loading system at sector 13²² of the Advanced Photon Source (APS). The XAFS data (Fe K-edge) were collected up to 15 GPa at 20-ID, APS. The data were processed with the program Athena and fitted with Artemis²³ with a similar procedure as that reported in the literature,²⁴ but with k -range 2–13.8 \AA^{-1} used.

RESULTS AND DISCUSSION

In Situ Neutron Diffraction. The bonding process in the O1–O2 phase transition can be understood by determining the variation of the atomic distances between Fe, C, and N. The crystal structures of $\text{K}_3\text{Fe}(\text{CN})_6$ before and after the phase transition (at 1.7 and 4.4 GPa, respectively) were determined by Rietveld refinement with the *in situ* neutron diffraction data (Figures S1 and S2). The refinement results indicate the a -axis has the highest compressibility while the b -axis is elongated after the O1–O2 phase transition, similar as that determined by XRD.¹⁹ The atomic coordinates as well as selected atomic distances and bond angles of $\text{K}_3\text{Fe}(\text{CN})_6$ refined under 1.7 and 4.4 GPa are shown in Tables S1–S4, and the corresponding structure is shown in Figure 1. At 1.7 GPa the phase O1 still

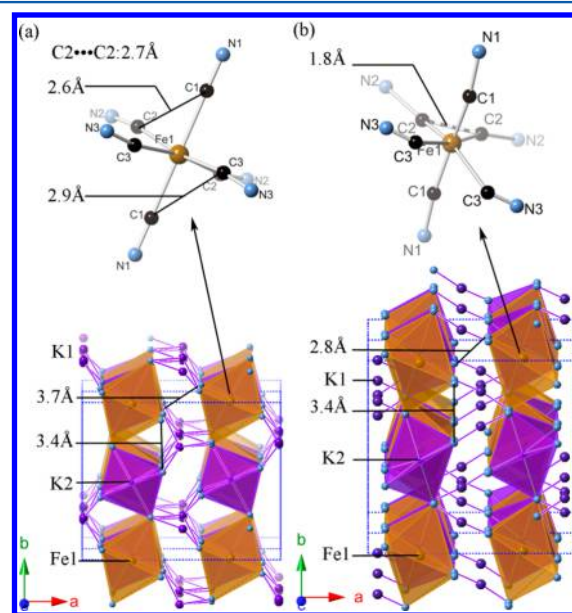


Figure 1. (a) Crystal structure of $\text{K}_3\text{Fe}(\text{CN})_6$ and local structure of $\text{Fe}(\text{CN})_6^{3-}$ under 1.7 GPa and (b) 4.4 GPa. The violet and brown octahedra stand for KN_6 and $\text{Fe}(\text{CN})_6$ octahedra in the layer, respectively. C atom is omitted in the octahedra for clarity.

maintains the layered structure, similar as that in ambient pressure. The $\text{KFe}(\text{CN})_6$ layer is formed by corner-sharing chains, which are constructed by alternating edge-sharing $\text{Fe}(\text{CN})_6^{3-}$ octahedra and KN_6 octahedra (K2), and the layers are separated by K cations (K1). The $\text{Fe}(\text{CN})_6^{3-}$ is distorted slightly at 1.7 GPa. The nearest interlayer N...N distances decrease to around 3.7 Å from 3.8 Å at ambient pressure, and the neighbored C...C distances inside $\text{Fe}(\text{CN})_6^{3-}$ are in the range of 2.6–2.9 Å.

The crystal structure of phase O2 (4.4 GPa) was refined starting with the structural model of phase O1. As suggested by the EXAFS analysis mentioned later, in the three crystallographically independent Fe–C bonds, two of them have similar bond lengths which are shorter than the third one. After several tests, the bond length Fe–C1 = Fe–C2 is proposed, and the structural details are shown in Tables S3 and S4. As shown in Figure 1b, the phase O2 still maintains the layered structure. K1 is almost pressed into the $\text{KFe}(\text{CN})_6$ layer, and the $\text{Fe}(\text{CN})_6^{3-}$ complex anion is severely compressed along the *a*-axis. The interlayer neighbored N...N distance is dramatically compressed to 2.8 Å from 3.7 Å, but still not covalently bonded.

Inside the $\text{Fe}(\text{CN})_6^{3-}$ complex anion, the distance of Fe–C2 (and Fe–C1 due to the constraint) decreases dramatically, while the Fe–N2 distance increases slightly. Simultaneously, the C2–C2 distance decreases to ~1.8 Å. This distance is 35% below the C2–C2 distance at ambient pressure (2.7 Å)²⁵ and significantly below the sum of van der Waals radius (~3.4 Å in solid HCN at ambient pressure and low temperature²⁶ and in NaCN at 4 GPa and room temperature⁸) and longer than the typical C–C single bond (1.54 Å). This indicates the two C2N2 anions inside $\text{Fe}(\text{CN})_6^{3-}$ react in the O1–O2 phase transition and result in a special coordination state with Fe(III). In such a state the C2...C2 atoms are weakly bonded, and the C2N2 triple bonds are greatly weakened and elongated, which is consistent with the decreasing Raman signal of the CN stretching mode in our previous study.¹⁹

Neutron Pair Distribution Function. The structure of $\text{K}_3\text{Fe}(\text{CN})_6$ becomes more disordered and finally amorphous when pressure is increased. The neutron PDF is used to study the local structure of the recovered $\text{K}_3\text{Fe}(\text{CN})_6$, which gives the likelihood of finding an atom at a given radius from another atom at an arbitrary origin.²⁷ *In situ* neutron PDF measurements under high pressure are extremely difficult, so $\text{K}_3\text{Fe}(\text{CN})_6$ samples recovered from high pressure were studied (Figure 2). The PDF ($G(r)$) patterns of samples recovered below 8 GPa are very similar to that of the initial material (0 GPa), which indicates the O1–O2 phase transition is reversible. The ordering range decreases to ~20 Å for the samples recovered from above 9 GPa, suggesting the O2–O3 phase transition is irreversible. The samples recovered from 13 to 20 GPa show an even shorter ordering range (less than 8 Å), indicating a complete irreversible amorphization.

A detailed examination of the first peak (carbon–nitrogen bond) is shown in Figure 2b. From 0 to 8 GPa, the peak remains near 1.15 Å, which is ascribed to the $\text{C}\equiv\text{N}$ triple bond. Upon further compression (9–20 GPa), the peak moves to greater radial distances, 1.18 Å at 20 GPa. Also, a shoulder at ~1.36 Å ($\text{C}=\text{N}^-$) is observed, which is more pronounced in the difference curve (Figure 2c). Comparing with the qualitative proof in the Raman spectra in our previous study,¹⁹ this is a convincing signature of a significant amount of $\text{C}=\text{N}$ double bonds, which evidence the reaction between cyanide anions. The continuous shifting of the C–N peak also indicates that

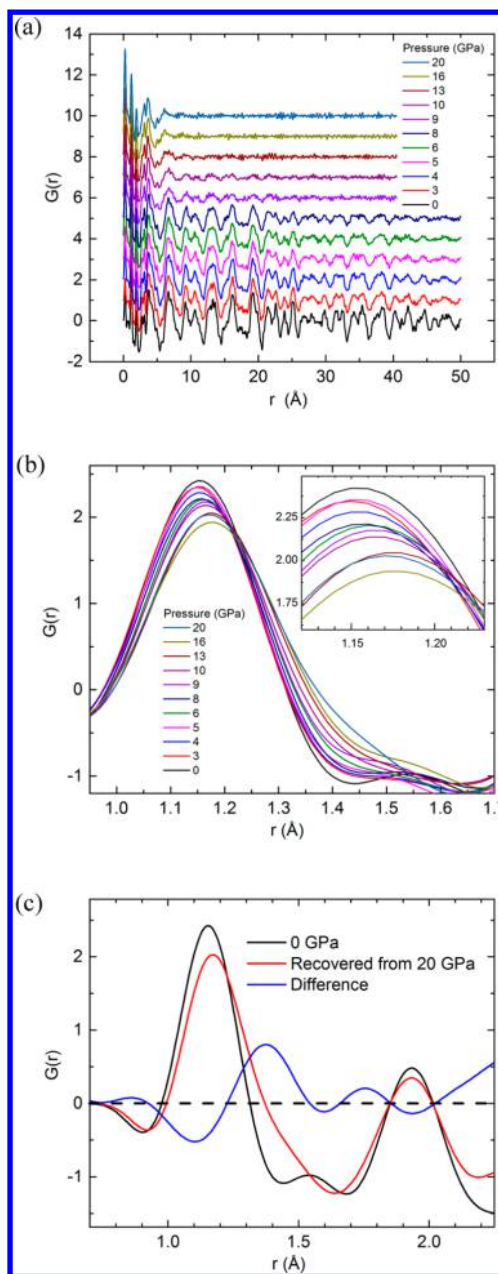


Figure 2. Neutron pair distribution functions ($G(r)$) of $\text{K}_3\text{Fe}(\text{CN})_6$ recovered from external pressures. (a) $G(r)$ up to 50 Å. (b) First peak of the $G(r)$, corresponding to the carbon–nitrogen bonds. (c) Difference between $G(r)$ of sample recovered from 20 GPa and that of raw material (0 GPa).

the irreversible reaction between the cyanide anions proceeds with increasing pressure.

The result from the PDF analysis is in consistency with the color of the samples (Figures S3 and S4). The samples recovered from 4 and 6 GPa are still yellow, while the samples recovered from 9 and 20 GPa are black and with small shiny particles (20 GPa). The change of color suggests that the reaction at 8 GPa is not reversible, and the samples recovered from pressure above 8 GPa have much smaller band gap, which is most likely attributed to the conjugated π -system. The 4–9 GPa samples are soluble in water. The solutions of sample recovered from 4 and 6 GPa are yellow, and the solution of that recovered from 9 GPa is colorless, probably because the Fe^{3+} is reduced to Fe^{2+} . The sample recovered from 20 GPa cannot

dissolve in water completely, forming dark-brown suspension. This suggests the irreversible bonding between the cyanides continues when pressure is increased above 9 GPa, and the sample recovered from 20 GPa already has a considerable degree of polymerization, which is important for applications on the cathode materials.

X-ray Absorption (XAFS). The structural analysis by neutron scattering raised the question of why the reaction is reversible in the O1–O2 transition but irreversible in the O2–O3 transition. Since *in situ* neutron diffraction data cannot support good refinement for phase O3, we employed *in situ* XAFS to study the local structure around Fe atom under high pressure. The selected Fourier transformed EXAFS spectra of Fe K-edge are shown in Figure 3. The peaks between 1.1 and

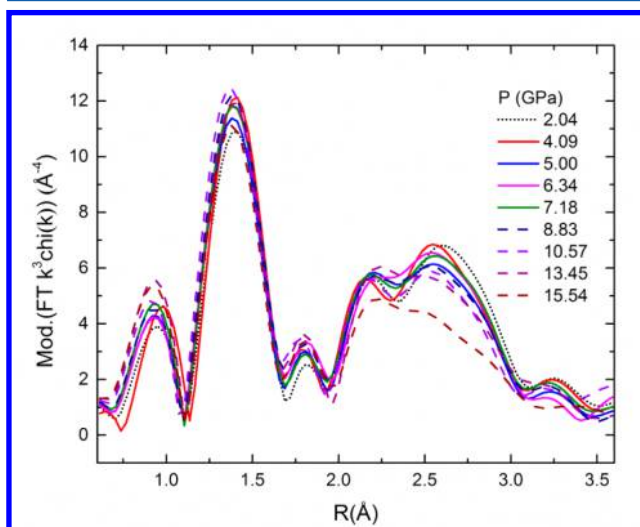


Figure 3. *In situ* Fourier transformed EXAFS spectra (moduli) of Fe K-edge of $\text{K}_3\text{Fe}(\text{CN})_6$ under high pressure.

1.8 Å correspond to the first coordination shell (Fe–C), and those between 2.0 and 3.0 Å correspond to the second shell (Fe–N) and multiple scatterings (Fe–N–C–Fe and Fe–C–N–C–Fe). Under external pressure the peak below 1.8 Å moves to low *r* slightly, indicating the first shell is compressed only a little. This means Fe maintains its 6-fold coordination through phase O2 (consistent with neutron diffraction), O3, and the amorphous phase. The second shell changes dramatically, which is attributed to the distortion of the Fe–C–N connection and probably the variation of C–N bonds. From 2 to 4 GPa, the second shell is compressed, while from 4 to 8 GPa the spectra remain nearly unchanged. Above 8 GPa, the second shell is compressed again and distorted dramatically. These two variations correspond to the phase transitions from phase O1 to O2 and O2 to O3 exactly.

To get more structural information, quantitative fitting was performed using the software Artemis.²³ Because of the distortion of the $\text{Fe}(\text{CN})_6^{3-}$ complex ion, the fitting of the EXAFS data was difficult when the second coordination shell (nitrogen and probably potassium) is considered. However, to get a convincing fitting of the first shell, we extend the cutting value to include all the second coordination shell to prevent any effect on the first coordination shell. The details are not discussed here. The results show the bond lengths of Fe–C1 and Fe–C2 converge to the same value, which is shorter than that of Fe–C3. This feature is employed as a constraint in the refinement of neutron diffraction data, as mentioned earlier.

For the data above 8 GPa (phase O3 and the amorphous phase), the fitting cannot reach a reasonable convergence. This may result from the inhomogeneous local environment of Fe through the whole sample after two phase transitions, which cannot be well fit by a single model.

Pre-Edge Region. The pre-edge region of the absorption curve (Figure 4) provides information on the oxidation state

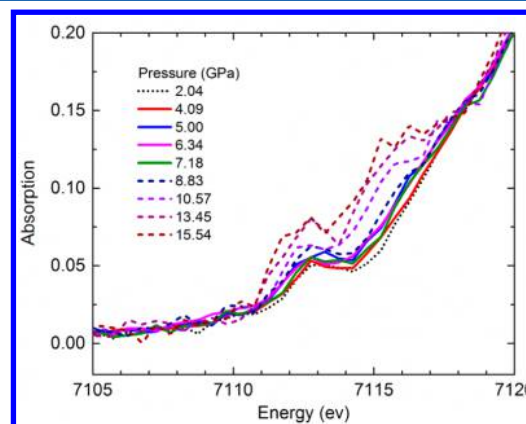


Figure 4. Pre-edge region of XAFS spectra of $\text{K}_3\text{Fe}(\text{CN})_6$ under high pressure.

and coordination geometry of Fe.^{28,29} At 2.04 GPa, the absorption peak at 7113 eV clearly indicates that Fe is trivalent, in a low-spin state, and has an octahedral coordination. This absorption curves are almost unchanged until 8 GPa. Above 8 GPa, two peaks rise at 7112 and 7115 eV. This is attributed to the presence of Fe(II) in octahedral coordination, similar to that of $\text{K}_4\text{Fe}(\text{CN})_6$ and several other octahedrally coordinated low-spin Fe(II) complexes. The peak at 7113 eV is also enhanced, which indicates a stronger 3d–4p mixing, suggesting the coordination of Fe is not perfectly octahedral but less centrosymmetric. This reduction process is similar to that reported in iron(III) halides, thiocyanate, and potassium ferricyanide.^{30–32}

The variations of $\text{K}_3\text{Fe}(\text{CN})_6$ under high pressure are summarized in Table 1. Combining with the above analysis,

Table 1. Summary of the Phase Transitions of $\text{K}_3\text{Fe}(\text{CN})_6$ under High Pressure

	O1	O2	O3	amor
color of recovered sample	yellow	yellow	black	black
color of aqueous solution	yellow	yellow	light	dark brown suspension
bonding of CN	$\text{C}\equiv\text{N}$	$\text{C}=\text{N}+\text{C}\equiv\text{N}$	$\text{C}=\text{N}$	$\text{C}=\text{N}$
oxidation state of Fe	+3	+3	+2	+2
σ (S cm^{-1}) ¹⁹	10^{-7}	10^{-4}	10^{-6}	10^{-6}
reversible to O1		yes	no	no

we can understand the PIP of $\text{K}_3\text{Fe}(\text{CN})_6$, and its effect on the conductivity more clearly. The O1–O2 transition is mainly because K1 is pressed into the $\text{KFe}(\text{CN})_6$ layer and the cyanide anions (C_2N_2) coordinating to the same Fe atom bond to each other. The O2–O3 transition is owing to the electron transfer from cyanide anions to Fe(III) and the following reactions

between CN^- . The reaction between (part of) CN^- is irreversible only after the electron transfer to Fe(III) , which suggests that reducing the charge density of the monomers is a useful method to prepare recoverable polymerized sample.

The PIP starts from the bonding of atoms coordinating to the same Fe(III) at a relatively low pressure instead of atoms bonding to the same K^+ . This is consistent with that the PIP of Prussian blue starts at a much lower pressure compared with the PIP of ACN ($\text{A} = \text{alkaline metal}$). The difference can be attributed to the different bonding of Fe-C and K-N . Fe(III) is much smaller than K^+ , and the Fe-CN coordination bonds are directional. Before compression the two carbon atoms are brought much closer ($\sim 2.7 \text{ \AA}$) than the two neighbored nitrogen atoms ($\sim 4 \text{ \AA}$), which makes the reaction between the carbon atoms much easier. The distance between the atoms is a key factor in the solid state reaction, as was reported in the literature.³³

The variation of the conductivity under external pressure reported in our previous study¹⁹ now can be interpreted on a structural basis. In $\text{K}_3\text{Fe(CN)}_6$ the resistance is mainly from the gap between neighbored Fe(CN)_6^{3-} . There are two types of neighboring, intralayer and interlayer, separated by K2 and K1 , respectively. At ambient pressure the interlayer $\text{N}\cdots\text{N}$ distance is $\sim 4 \text{ \AA}$, much bigger than the intralayer $\text{N}\cdots\text{N}$ distance (3.4 \AA); therefore, the interlayer gap is the bottleneck for the electron conduction. In the first phase transition (O1 to O2), the interlayer space is dramatically compressed, and K1 is almost pressed into the layer. The distances between the interlayer neighbored CN^- decrease from ~ 4 to $\sim 2.8 \text{ \AA}$, while that of the intralayer neighbored Fe(CN)_6^{3-} is still about 3.4 \AA . The 2.8 \AA observed in the interlayer neighbored CN^- is smaller than the sum of van der Waals radii of nitrogen (3.1 \AA), which indicates significant overlap of orbitals. Hence we can conclude that the decreasing of the interlayer distance is the predominant reason for the 10^3 -fold enhancement of the electronic conductivity. A second reason most likely results from the structural variation inside the Fe(CN)_6^{3-} complex ion, mainly the distortion of Fe(CN)_6^{3-} and the bonding between the CN^- . These structural variations build up a conducting circuit in the crystal structure of phase O2 , as shown in Figure 5.

The decrease of electronic conductivity at the O2-O3 phase transition is accompanied by the transition of Fe(III) to Fe(II) and the irreversible reaction between CN^- . In phase O2 , the two reacted CN^- approaches each other under higher external

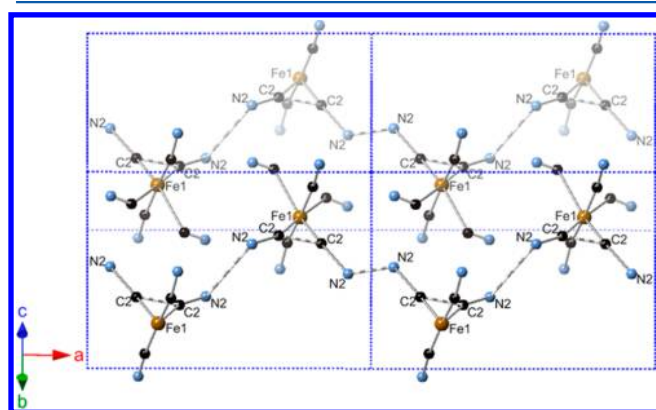


Figure 5. Conducting circuit in the O2 phase of $\text{K}_3\text{Fe(CN)}_6$ under 4.4 GPa . The conducting circuit is along the N2-C2-(Fe)-C2-N2 atoms.

pressure, and at around 8 GPa , an electron is squeezed out to Fe(III) . The charge density on the cyanides is hence decreased as is the repulsive forces between groups, resulting in a more stable chemical bond. The decrease of the conductivity is most likely because the crystal lattice is interrupted by the irreversible bonding, and the electron conducting circuit is destroyed to some extent. Another possible reason may come from the reduction of Fe(III) to a close shell cation Fe(II) and the oxidation of the CN network.

CONCLUSIONS

By determining the crystal structure and the electronic structure of $\text{K}_3\text{Fe(CN)}_6$ under high pressure, the PIP process is well understood and can be divided into three steps. (1) Approaching. Compared with K^+ , Fe(III) brought the coordinating CN close to each other, which facilitates the bonding between carbon atoms. The approach of Fe(CN)_6^{3-} from neighboring layers forms a conducting circuit and results in the 10^3 -fold enhancement of conductivity. (2) Bonding. Above $2-4 \text{ GPa}$ two cyanide anions of the same Fe(CN)_6^{3-} form a weak bond reversibly between the carbon atoms. (3) Stabilizing. At $7-8 \text{ GPa}$, the Fe(III) is reduced to Fe(II) by the cyanide anions, which stabilizes the bonds between CN and makes it recoverable to ambient pressure. The research clearly indicates that transition metals, in place of alkali metals, can help unsaturated anions to polymerize at lower pressure by bringing them closer and decreasing their charge density, making the PIP of charged monomers occur more easily. The transition metal actually acts as a catalyst. Our finding provides a clear understanding of the reaction mechanism of CN^- on the microscopic scale, which paves a way to designing and synthesizing new materials with PIP reactions. The reduction of Fe^{3+} by CN also demonstrates the oxidation/reduction activity of this system, which sheds light on its potential application for cathode materials of alkali metal battery.

ASSOCIATED CONTENT

Supporting Information

The Supporting Information is available free of charge on the ACS Publications website at DOI: 10.1021/acs.jpcc.5b06793.

Atomic coordinates and selected bond length and angles of $\text{K}_3\text{Fe(CN)}_6$ under high pressure (PDF)

AUTHOR INFORMATION

Corresponding Authors

*(K.L.) E-mail likuo@hpstar.ac.cn.

*(H.Z.) E-mail zhenghy@hpstar.ac.cn.

Funding

This work was partially supported as part of the Energy Frontier Research in Extreme Environment (EFREE) Center, an Energy Frontier Research Center funded by Basic Energy Sciences (BES), Department of Energy (DOE), under Award DE-SC0001057. Wenge Yang and Ho-kwang Mao acknowledge the financial support from DOE-BES X-ray Scattering Core Program under Grant DE-FG02-99ER45775.

Notes

The authors declare no competing financial interest.

ACKNOWLEDGMENTS

The authors thank Dr. Dale L. Brewe for XAFS data collection and Dr. Mahalingam Balasubramanian for discussions. A

portion of this research at Oak Ridge National Laboratory's Spallation Neutron Source was sponsored by the Scientific User Facilities Division, Office of Basic Energy Sciences (BES), U.S. Department of Energy (DOE). SNAP is highly acknowledged for the *in situ* neutron diffraction and sample synthesis. The authors acknowledge the support of NSFC (Grant No: U1530402).

REFERENCES

- (1) Gou, H.; Yonke, B. L.; Epshteyn, A.; Kim, D. Y.; Smith, J. S.; Strobel, T. A. Pressure-Induced Polymerization of P(CN)₃. *J. Chem. Phys.* **2015**, *142*, 194503–1–9.
- (2) Wilhelm, C.; Boyd, S. A.; Chawda, S.; Fowler, F. W.; Goroff, N. S.; Halada, G. P.; Grey, C. P.; Lauher, J. W.; Luo, L.; Martin, C. D.; et al. Pressure-Induced Polymerization of Diiodobutadiene in Assembled Cocystals. *J. Am. Chem. Soc.* **2008**, *130*, 4415–4420.
- (3) Evans, W. J.; Lipp, M. J.; Yoo, C. S.; Cynn, H.; Herberg, J. L.; Maxwell, R. S.; Nicol, M. F. Pressure-Induced Polymerization of Carbon Monoxide: Disproportionation and Synthesis of an Energetic Lactonic Polymer. *Chem. Mater.* **2006**, *18*, 2520–2531.
- (4) Chelazzi, D.; Ceppatelli, M.; Santoro, M.; Bini, R.; Schettino, V. Pressure-Induced Polymerization in Solid Ethylene. *J. Phys. Chem. B* **2005**, *109*, 21658–21663.
- (5) Talyzin, A. V.; Dubrovinsky, L. S.; Le Bihan, T.; Jansson, U. Pressure-Induced Polymerization of C₆₀ at High Temperatures: An *in Situ* Raman Study. *Phys. Rev. B: Condens. Matter Mater. Phys.* **2002**, *65*, 245413–1–10.
- (6) Fitzgibbons, T. C.; Guthrie, M.; Xu, E.-s.; Crespi, V. H.; Davidowski, S. K.; Cody, G. D.; Alem, N.; Badding, J. V. Benzene-Derived Carbon Nanowires. *Nat. Mater.* **2015**, *14*, 43–47.
- (7) Murlu, C.; Song, Y. Pressure-Induced Polymerization of Acrylic Acid: A Raman Spectroscopic Study. *J. Phys. Chem. B* **2010**, *114*, 9744–9750.
- (8) Chen, J. Y.; Yoo, C. S. Physical and Chemical Transformations of Sodium Cyanide at High Pressures. *J. Chem. Phys.* **2009**, *131*, 144507–1–7.
- (9) Heckathorn, J. W.; Kruger, M. B.; Gerlich, D.; Jeanloz, R. High-Pressure Behavior of the Alkali Cyanides KCN and NaCN. *Phys. Rev. B: Condens. Matter Mater. Phys.* **1999**, *60*, 979–983.
- (10) Li, Y. L.; Luo, W.; Zeng, Z.; Lin, H. Q.; Mao, H. K.; Ahuja, R. Pressure-Induced Superconductivity in CaC₂. *Proc. Natl. Acad. Sci. U. S. A.* **2013**, *110*, 9289–9294.
- (11) Efthimiopoulos, I.; Kunc, K.; Vazhenin, G. V.; Stavrou, E.; Syassen, K.; Hanfland, M.; Liebig, S.; Ruschewitz, U. Structural Transformation and Vibrational Properties of BaC₂ at High Pressure. *Phys. Rev. B: Condens. Matter Mater. Phys.* **2012**, *85*, 054105–1–9.
- (12) Asakura, D.; Li, C. H.; Mizuno, Y.; Okubo, M.; Zhou, H.; Talham, D. R. Bimetallic Cyanide-Bridged Coordination Polymers as Lithium Ion Cathode Materials: Core@Shell Nanoparticles with Enhanced Cyclability. *J. Am. Chem. Soc.* **2013**, *135*, 2793–2799.
- (13) Lu, Y. H.; Wang, L.; Cheng, J. G.; Goodenough, J. B. Prussian Blue: A New Framework of Electrode Materials for Sodium Batteries. *Chem. Commun.* **2012**, *48*, 6544–6546.
- (14) Strössner, K.; Hochheimer, H. D.; Hönle, W.; Werner, A. High-Pressure Raman and X-Ray Studies of the Alkali Cyanides up to 27 GPa. *J. Chem. Phys.* **1985**, *83*, 2435–2440.
- (15) Liu, X. J.; Moritomo, Y.; Matsuda, T.; Kamioka, H.; Tokoro, H.; Ohkoshi, S. Pressure-Induced Octahedral Rotation in RbMn[Fe(CN)₆]. *J. Phys. Soc. Jpn.* **2009**, *78*, 013602–1–4.
- (16) Matsuda, T.; Liu, X. J.; Shibata, T.; Kamioka, H.; Ohishi, Y.; Moritomo, Y. Pressure-Induced Phase Transition in Zn-Fe Prussian Blue Lattice. *J. Phys. Soc. Jpn.* **2009**, *78*, 105002–1–2.
- (17) Catafesta, J.; Haines, J.; Zorzi, J. E.; Pereira, A. S.; Perottoni, C. A. Pressure-Induced Amorphization and Decomposition of Fe[Co(CN)₆]. *Phys. Rev. B: Condens. Matter Mater. Phys.* **2008**, *77*, 064104–1–5.
- (18) Moritomo, Y.; Hanawa, M.; Ohishi, Y.; Kato, K.; Takata, M.; Kuriki, A.; Nishibori, E.; Sakata, M.; Ohkoshi, S.; Tokoro, H.; et al. Pressure- and Photoinduced Transformation into a Metastable Phase in RbMn[Fe(CN)₆]. *Phys. Rev. B: Condens. Matter Mater. Phys.* **2003**, *68*, 144106–1–7.
- (19) Li, K.; Zheng, H.; Ivanov, I. N.; Guthrie, M.; Xiao, Y.; Yang, W.; Tulk, C. A.; Zhao, Y.; Mao, H. K₃Fe(CN)₆: Pressure-Induced Polymerization and Enhanced Conductivity. *J. Phys. Chem. C* **2013**, *117*, 24174–24180.
- (20) Klotz, S.; Hamel, G.; Frelat, J. A New Type of Compact Large-Capacity Press for Neutron and X-Ray Scattering. *High Pressure Res.* **2004**, *24*, 219–223.
- (21) Neufeind, J.; Feygenson, M.; Carruth, J.; Hoffmann, R.; Chipley, K. K. The Nanoscale Ordered Materials Diffractometer Nomad at the Spallation Neutron Source SNS. *Nucl. Instrum. Methods Phys. Res., Sect. B* **2012**, *287*, 68–75.
- (22) Rivers, M.; Prakapenka, V. B.; Kubo, A.; Pullins, C.; Holl, C. M.; Jacobsen, S. D. The Compres/Gsecars Gas-Loading System for Diamond Anvil Cells at the Advanced Photon Source. *High Pressure Res.* **2008**, *28*, 273–292.
- (23) Ravel, B.; Newville, M. Athena, Artemis, Hephaestus: Data Analysis for X-Ray Absorption Spectroscopy Using Iffit. *J. Synchrotron Radiat.* **2005**, *12*, 537–541.
- (24) Baldini, M.; Yang, W.; Aquilanti, G.; Zhang, L.; Ding, Y.; Pascarelli, S.; Mao, W. L. High-Pressure EXAFS Measurements of Crystalline Ge Using Nanocrystalline Diamond Anvils. *Phys. Rev. B: Condens. Matter Mater. Phys.* **2011**, *84*, 014111–1–5.
- (25) Figgis, B. N.; Skelton, B. W.; White, A. H. Crystal-Structures of Simple Monoclinic and Orthorhombic Polytypes of Tripotassium Hexacyanoferrate(III). *Aust. J. Chem.* **1978**, *31*, 1195–1199.
- (26) Dulmage, W. J.; Lipscomb, W. N. The Crystal Structures of Hydrogen Cyanide, HCN. *Acta Crystallogr.* **1951**, *4*, 330–334.
- (27) Billinge, S. J. L.; Kanatzidis, M. G. Beyond Crystallography: the Study of Disorder, Nanocrystallinity and Crystallographically Challenged Materials with Pair Distribution Functions. *Chem. Commun.* **2004**, 749–760.
- (28) Hayakawa, K.; Hatada, K.; D'Angelo, P.; Della Longa, S.; Natoli, C. R.; Benfatto, M. Full Quantitative Multiple-Scattering Analysis of X-Ray Absorption Spectra: Application to Potassium Hexacyanoferrate(II) and -(III) Complexes. *J. Am. Chem. Soc.* **2004**, *126*, 15618–15623.
- (29) Westre, T. E.; Kennepohl, P.; DeWitt, J. G.; Hedman, B.; Hodgson, K. O.; Solomon, E. I. A Multiplet Analysis of Fe K-Edge 1s → 3d Pre-Edge Features of Iron Complexes. *J. Am. Chem. Soc.* **1997**, *119*, 6297–6314.
- (30) Lewis, G. J.; Whalley, E. Supposed Pressure-Induced Reduction of Ferric Salts. *J. Chem. Phys.* **1980**, *72*, 2291–2294.
- (31) Drickamer, H. G.; Lewis, G. K.; Fung, S. C. Oxidation State of Iron at High Pressure. *Science* **1969**, *163*, 885–890.
- (32) Fung, S. C.; Drickamer, H. G. Effect of Pressure on C-Fe Bond in Ferrocyanides and Ferricyanides. *J. Chem. Phys.* **1969**, *51*, 4353–4359.
- (33) Varga, K.; Volaric, J.; Vancik, H. Crystal Disorder and Organic Solid-State Reactions. *CrystEngComm* **2015**, *17*, 1434–1438.